Space group and atomic structure determination of a nano-sized ordered phase derived from a f.c.c. structure in maraging steel 12Cr–9Ni–4Mo–2Cu using transmission electron microscopy

Ping Liu

Department of Physical Metallurgy, Research and Development Centre, Sandvik Materials Technology, SE-811 81 Sandviken, Sweden

Correspondence e-mail: ping.liu@sandvik.com

The unique properties of maraging steel Sandvik 1RK91 were attributed to unique precipitation: a nano-sized L phase in addition to the quasi-crystalline R' phase, which differs from any precipitation system in conventional maraging steels. The L phase was observed after ageing at either 748 or 823 K. It has flake morphology with dimensions $\sim 100 \times 500 \times 500$ Å. In the present study the structure of the L phase was examined using convergent-beam electron diffraction (CBED), energy-dispersive X-ray analysis (EDX) and high-resolution electron microscopy (HREM). The L phase could be described as $Ti_{19}Fe_9Mo_9Al_8Cr_5Ni_{50}$ or simply $M_{50}Ni_{50}$ (M = Ti, Fe, Mo, Al and Cr). The L phase is isostructural to FeNi. Its crystal structure was determined to have the ordered structure of the uAu-I type ($L1_0$, $P4/mmm$, $a = 3.52$, $c = 3.63$ Å and $Z = 2$) with two Ni atoms at $\frac{1}{2}\,0\,\frac{1}{2}$ and $0\,\frac{1}{2}\,\frac{1}{2}$, and two M atoms at $0\,0\,0$ and $\frac{1}{2}\,\frac{1}{2}\,0$. The crystal structure of the L phase can also be described using a primitive tetragonal cell and lattice parameters: $a = 2.49$ and $c = 3.63$ Å, $Z = 1$. The volume of the primitive tetragonal unit cell is 22.5 $Å^3$ and the density is ~ 6.98 g cm^{-3}. The present study has demonstrated the possibility of determining the structure of an extremely small crystal by utilizing the information from CBED, EDX analysis and HREM.

1. Introduction

Maraging steels have a combination of ultra-high strength and a high level of toughness (Floreen, 1968). The ultra-high strength and high toughness are attributed to a combination of the martensitic transformation during air cooling after solution heat treatment at a temperature between 1073 and 1273 K in the austenite region and precipitation in the cubic martensitic matrix during subsequent ageing at a temperature between 673 and 973 K (Floreen, 1968; Deckers & Floreen, 1988).

Maraging steels generally have a low concentration of carbon (about 0.01 wt %), about 18 wt % nickel and substantial amounts of cobalt and molybdenum and smaller additions of titanium, which promote precipitation-hardening reactions when the solution-treated steels are aged.

The types of precipitation depend upon the composition and the exact ageing temperature. The reported precipitates have been summarized by Floreen (1968) and Deckers & Floreen (1988). The main precipitates found in the maraging

Table 1
The chemical composition of the experimental sample Sandvik 1RK91 (wt %).

Cr	Ni	Mo	Cu	Ti	Al	Mn	Si	C	Fe
12.20	8.99	4.02	1.95	0.87	0.33	0.32	0.15	0.01	71.16

Table 2
Heat treatments of the materials studied.

Solution heat treatment	Followed ageing
1323–1423 K with subsequent air-cooling	748 K for 1000 h followed by air-cooling
1323–1423 K with subsequent air-cooling	748 + 823 K for 100 h followed by air-cooling
1323–1423 K with subsequent air-cooling	823 + 748 K for 100 h followed by air-cooling
1323–1423 K with subsequent air-cooling	823 K for 400 h followed by air-cooling

steels are: Ni_3M (M = V, Mo, Nb) with either orthorhombic or close-packed hexagonal structure; η-Ni_3Ti with $D0_{24}$ ordered hexagonal structure; Fe_2Mo Laves phase; the σ phase of different types (FeMo, FeTi); μ-Fe_7Mo_6; and the χ phase. The rhombohedral R phase was also found but is less common. η-Ni_3Ti was found to precipitate at an early stage of ageing in both Co-containing and Co-free alloys (Floreen, 1968; Deckers & Floreen, 1988; Kim *et al.*, 1988; Vasudevan *et al.*, 1990; Sha *et al.*, 1993*a,b*). However, during prolonged ageing, orthorhombic Ni_3W precipitated in a W-containing alloy (Kim *et al.*, 1988); the Fe_2Mo Laves phase was found to have precipitated in the low cobalt-containing alloy (Vasudevan *et al.*, 1990), and the μ-Fe_7Mo_6 phase was formed in both cobalt-containing and -free alloys (Sha *et al.*, 1993*a,b*). In addition to these, a ω phase and G-$Ti_6Si_7Ni_{16}$ silicide were also found to precipitate in Cr-containing maraging steel (Viswanathan *et al.*, 1993). The precipitation of η-Ni_3Ti was reported to have heterogeneous nucleation on the dislocation in maraging steel (Sha *et al.*, 1993*c*).

The recently developed maraging steel 12Cr–9Ni–4Mo designated as Sandvik 1RK91 (in the following termed Sandvik 1RK91) is intended for the applications that require a combination of high strength, ductility and corrosion resistance, such as surgical needles and dental instruments, which have complicated shapes and are often used in a very corrosive environment. This steel has shown an unusual tempering response, high strength and ductility, corrosion resistance and high resistance against overageing, the combination of which is unique (Hultin Stigenberg & Nilsson, 1993; Liu *et al.*, 1994). The strong tempering response in the new steel can be as high as 1000 MPa. A final strength is attainable in the upper end of the specified interval 2500–3000 MPa.

The anomalous tempering response after ageing at 748 K, combined with high strength, ductility, corrosion resistance and a high resistance to overageing were attributed to the formation of a quasicrystalline phase, designated as the R' phase (Liu *et al.*, 1994). An additional ordered phase designated the L phase precipitated during prolonged ageing. Owing to its nano-size and its co-existence with other types of precipitates it is very difficult to determine the crystal struc-

ture using X-ray diffraction. The structure of this phase was determined using convergent-beam electron diffraction (CBED), combined with energy-dispersive X-ray analyses (EDX) and high-resolution electron microscopy (HREM).

2. Experimental

The chemical composition of the experimental sample of Sandvik 1RK91 maraging stainless steel used in this study is given in Table 1.

The sample of Sandvik 1RK91 steel for the present investigation was produced as wire from a full scale 7 ton melt followed by drawing with a 91% area production to a final diameter of 0.9 mm. The sample was then solution heat treated at 1323–1423 K with subsequent air-cooling. Different ageing (heat treatment to obtain precipitation strengthening) was then carried out. A summary of the heat treatments is given in Table 2.

Thin foils were electrochemically polished using an electrolyte of 15% perchloric acid in methanol at 17 V and 243 K.

In order to obtain both diffraction patterns without distortion due to the magnetic martensitic matrix and EDX analyses without the influence of the matrix, the precipitated particles were extracted using two methods: carbon replica and electro-chemical extraction. Carbon replicas were obtained by etching in a solution of 12.5 g $CuCl_2$ in 50 ml ethanol and 50 ml HCl and then coating with a thin layer of carbon. The replica containing the precipitated particles was stripped from the specimen by etching in 5% Br_2 and water-free methanol. In order to analyse the concentration of copper, carbon–nylon grids were used to support the carbon replicas.

Precipitated powders were extracted from the bulk by electrolytic dissolution of the matrix in a solution of 394 ml HCl in 1500 ml ethanol. A drop of the dispersion was placed on holey carbon film.

Thin foils, carbon replicas and the electro-chemical extracted residuals were then studied using a Jeol 2000-FX analytical transmission electron microscope (TEM/STEM) equipped with a Link AN 10,000 EDX system operating at 200 kV.

Electron diffraction intensities were extracted from the negatives of the diffraction patterns using the system ELD (Zou *et al.*, 1993, 1994).

3. Results

### 3.1. Determination of the unit cell and space group

A large number of nano-sized particles were observed after prolonged double ageing at 748 + 823 K for 100 h, as shown by both the bright field image (BF) in Fig. 1(*a*) and the centred-

dark field image (CDF) in Fig.1(*b*). This precipitate is termed the *L* phase. It can be seen that the particles have a flake morphology with dimensions ~100 × 500 × 500 Å. Furthermore, there are two sets of *L* phase particles, which are perpendicular to each other. The same type of particle was also observed in both samples aged at 823 K for 400 h (Fig. 2*a*) and aged at 748 K for 100 h (Fig. 2*b*), respectively.

A carbon replica of a sample aged at 748 K for 100 h is shown in Fig. 3(*a*). It can be seen that in addition to the quasicrystalline phase *R'* phase (Liu *et al.*, 1994), a number of *L* phase particles were observed, from which EDX analyses were performed without the influence of the matrix. A typical EDX spectrum is shown in Fig. 3(*b*). EDX analyses were carried out on ten particles of the *L* phase, which gave rise to the chemical analysis of the *L* phase: Ti 16.4 ± 1.4, Fe 8.5 ± 0.8, Mo 15.4 ± 1.9, Al 3.7 ± 1.1, Cr 4.4 ± 0.2, Ni 51.6 ± 2.5 in wt %. The conversion of weight per cent to mole per cent gave

rise to Ti 19.49 ± 2.9, Fe 8.67 ± 1.4, Mo 9.14 ± 1.9, Al 7.83 ± 4.1, Cr 4.82 ± 0.4, Ni 50.05 ± 4.3, in mol %. This phase therefore, could be described as $Ti_{19}Fe_9Mo_9Al_8Cr_5Ni_{50}$ or simply $M_{50}Ni_{50}$, where M = Ti, Fe, Mo, Al and Cr.

Using an electron beam of 200 Å, a series of tilting experiments of the *L* phase crystal resulted in a number of small-angle CBED patterns, five of which are shown in Fig. 4. The pattern in Fig. 4(*a*) reveals 4*mm* symmetry (Buxton *et al.*, 1976) and, therefore, the *L* phase could have either a cubic or a tetragonal structure. The patterns in Figs. 4(*b*)–(*e*) show two sets of diffraction spots: strong ones with the diffraction conditions $h + k, k + l, (l + h) = 2n$ (*n*: integer), corresponding to the face-centred Bravais lattice type, and weak ones with the diffraction conditions $h + k = 2n$ and no restriction on h (or k) + l. Thus, from the strong diffraction spots an f.c.c. structure could be recognized if a small deviation from cubic symmetry was neglected and the patterns could then be indexed as the
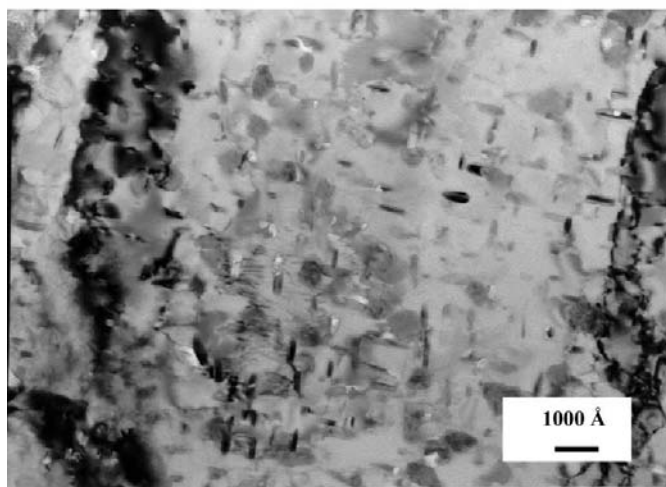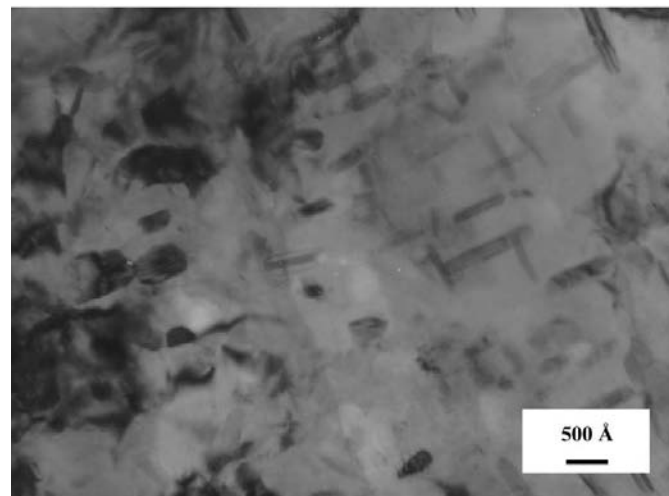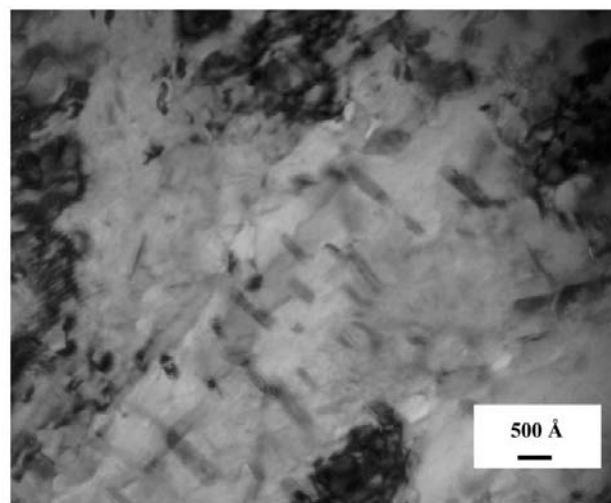

(*a*)
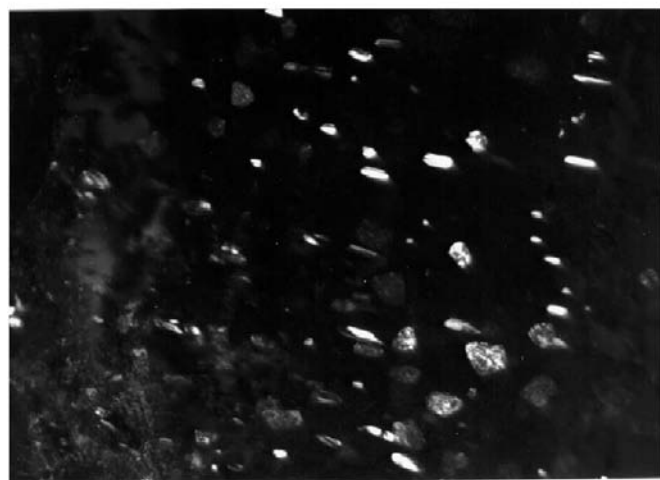
(*b*)

Figure 1
(*a*) Bright field image (BF) of precipitates of small nano-sized *L* phase particles with flake-like morphology and the dimensions 100 × 500 × 500 Å after prolonged ageing at 823 K for 100 h and 48 K for 100 h (thin foil). (*b*) Centred dark-field image (CDF) of the same area.
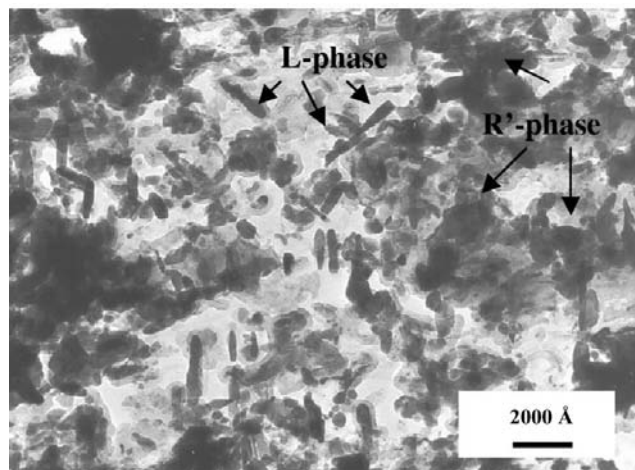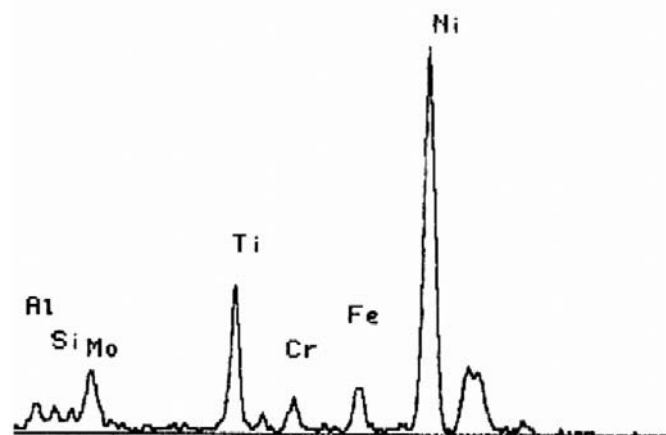

(*a*)

(*b*)

Figure 2
The *L* phase in a sample aged at 823 K for 400 h. (*b*). The *L* phase in a sample aged at 748 K for 100 h.

[001], [100], [111], [110] and [112] zone axes for Fig. 4(a)–(e), respectively (f.c.c. indexing is used throughout the paper because this structure was derived from f.c.c., as determined later). However, the 'extra' weak spots in the zone axes of [100] in Fig. 4(b), [111] in Fig. 4(c), [110] in Fig. 4(d) and [112] in Fig. 4(e) revealed the diffraction conditions of $h + k = 2n$, where h(or k) + l could be either even or odd, which are not consistent with an f.c.c. structure. The 'extra' weak spots indicate a long-range order in the crystal structure (Edington, 1975). The weak spots in the zone axis of [100] in Fig. 4(b) reduced the symmetry for the $\langle 100 \rangle$ pattern from $4mm$ for an f.c.c. crystal to $2mm$. Similarly, the symmetry of the [111] pattern was reduced from $3m$ for an f.c.c. to m (Fig. 4c). This means that the crystal system has changed. The pattern symmetry of [110] in Fig. 4(d) remains $2mm$. The point group of the L phase was deduced from the symmetries in the different zone axes (Buxton et al., 1976) and the L phase has a tetragonal structure with point group $(4/m)(2/m)(2/m)$-

(a)

(b)

$(4/m)\overline{3}(2/m)(m3m)$.

The appearance of {0kl} reflections with $k + l = 2n + 1$ in the [100] zone axis pattern in Fig. 4(b) and the [110] zone axis in Fig. 4(d) reveals that the L phase has a primitive Bravais lattice. The structure of the L phase, therefore, does not belong to any of the ordered structures with a non-primitive lattice. Hence, the L phase has a primitive tetragonal structure with a space group of $P4/mmm$, No. 123. The measurement of reflections {020} and {002} in the [100] zone axis in Fig. 4(b) revealed that the c axis is longer than the a axis. The lattice parameters were then determined to be $a = 3.52$ and $c = 3.63$ Å. This structure is, therefore, isostructural to FeNi, which has an ordered structure derived from an f.c.c. phase of type $A1$ (Cu) and $L1_0$ structure type (AuCu-I); space group $P4/mmm$ (No. 123) and lattice parameters of $a = 3.579$ and $c = 3.579$ Å (Danon et al., 1980).

Very often a micro-twin-like structure was observed, as shown in Fig. 5(a). The small-angle CBED pattern from this type of structure is shown in Fig. 5(b). It is noteworthy that extra reflections appear along the $(1\overline{1}1)$ direction (as indicated by the white arrow) between two fundamental reflections (indicated by the black arrows). The extra reflections are indeed due to the $(1\overline{1}1)$ twinning, as shown by the schematic solutions of the pattern in Fig. 5(c). The streaking shown along the $(1\overline{1}1)$ directions in Fig. 5(b) was attributed to the higher-order twinning.

3.2. Determination of the atomic positions

The L phase can be described as MNi, where Fe has been partially substituted by atoms of Ti, Mo, Al and Cr. The lattice parameters of the L phase differ from those of FeNi by less than 1.6%.

It is known that atoms can substitute partially for an atom with a much smaller radius in the structure. For example, Sr atoms partially substitute for both Ca and Pb in the $L1_0$ structure of CaPb (Villars & Calvert, 1985), although the atomic radius of Sr (2.15 Å) is more than 18% larger than that of Pb (1.75 Å; Vainshtein et al., 1982). It is therefore, possible that atoms with large radii, such as Ti, Mo, Al and Cr, could substitute for Fe atoms in the L phase structure. If the effective radius (r_M) is introduced as $r_M = \Sigma r_i \cdot A_i$, where A_i is the atomic percent of i atom, $r_{Ti} = 1.46$, $r_{Mo} = 1.39$, $r_{Al} = 1.43$, $r_{Cr} = 1.27$ and $r_{Fe} = 1.26$ Å, while $r_{Ni} = 1.24$ Å (Vainshtein et al., 1982), then $r_M = 0.130$ nm is obtained, which differs from that of Fe by only 3%.

Hence, the atomic model of the L-phase structure could be constructed based on partial substitution of Fe atoms in the FeNi structure (Danon et al., 1980), as shown in Fig. 6. Thus, two M atoms occupy the 0 0 0 and the $\frac{1}{2}\frac{1}{2}$ 0 positions and two Ni atoms occupy $\frac{1}{2}$ 0 $\frac{1}{2}$ and 0 $\frac{1}{2}\frac{1}{2}$, positions. The structure-factor F_{hkl} can then be calculated as

$$F_{hkl} = \begin{cases} 2[f_M + (-1)^{h+l}f_{Ni}], & \text{for } h + k = 2n; \\ 2[f_M + f_{Ni}], & \text{for } h \text{ (or } k) + l = 2n; \\ 2[f_M - f_{Ni}], & \text{for } h \text{ (or } k) + l = 2n + 1, n = 0, 1, 2, \dots \\ 0, & \text{for } h + k \neq 2n, n = 0, 1, 2, \dots \end{cases}$$

The electron diffraction amplitudes (intensities) can then be calculated. The atomic scattering amplitudes for each atom were taken from the literature (Wilson, 1995). The experimental intensities were measured from the negatives of diffraction patterns shown in Fig. 4 using the system ELD (Zou et al., 1993, 1994). The experimental intensities (I_{exp}) are listed in Table 3 together with the calculated ones (I_{calc}).

The reliability factor may be written as $R = \sum|I_{exp} - I_{calc}|/\sum|I_{exp}| = 0.38$ (Vainshtein, 1981). Thus, the calculated intensities match the experimental ones reasonably well. Thus, the structure of the L phase is the ordered structure type of $L1_0$ (AuCu-I) derived from the f.c.c. with the A1-type structure (Cu) and can be described as in Fig. 6. The unit cell of the L phase could be chosen as the smaller tetragonal cell indicated by the dashed line and the lattice parameters then become $a =$
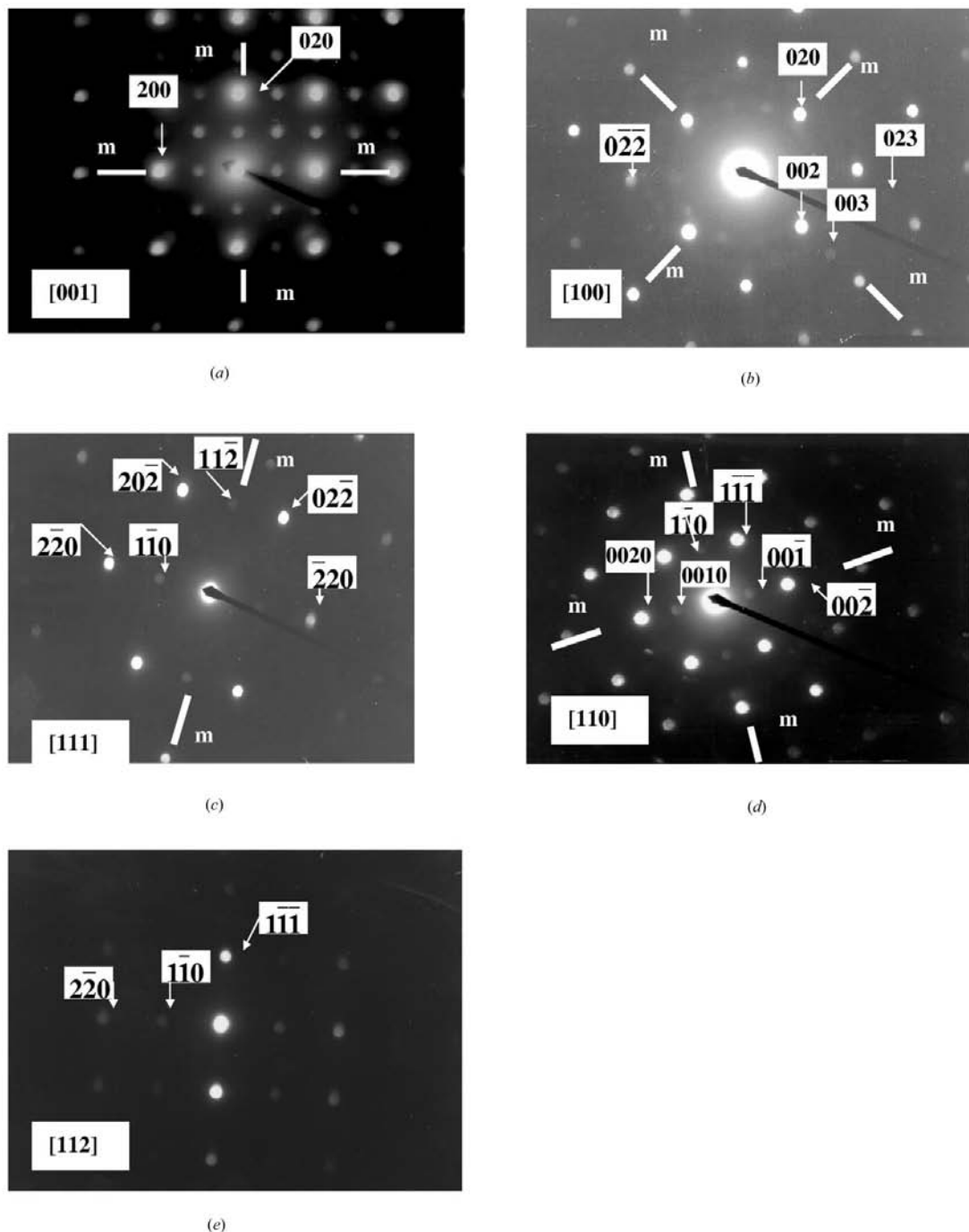

Figure 4
Small-angle CBED patterns from different zone axes of the L phase: (a) [001]; (b) [100]; (c) [111]; (d) [110]; (e) [112] zone axis of the L phase.

Ping Liu · Space group and atomic structure determination **171**

2.49 and c = 3.63 Å. The volume of the tetragonal unit cell could then be calculated as 22.5 Å^3 and the density as ~6.98 g cm^{-3}, Z = 1.

4. Discussion

The classical example of the ordered $L1_0$ phase is AuCu (Cullity, 1978). Its structure may be derived from the solid solution of the f.c.c., $Fm\overline{3}m$ structure with a structure of type $A1$, disordered AuCu. The ordering not only changes the Bravais lattice type (from face-centred to primitive), but also the crystal system (from cubic to tetragonal). However, the cubic cell has been used to derive the primitive tetragonal structure of $L1_0$ (ex. Cullity, 1978; Danon *et al.*, 1980; Villars & Calvert, 1985) for historical reasons. As a consequence the Bravais lattice type of the ordered structure would be the C lattice type with space group $C4/mmm$. This is only a different description of the same space group No. 123 (D_{4h}^1). Conventionally, Hermann–Mauguin symbols for the standard primitive cell is used, therefore, the ordered phase is described as $P4/mmm$. The point group of $4/mmm$ for $L1_0$ is a maximal

conjugate sub-group of $m\overline{3}m$ for the disordered f.c.c. $A1$ phase (van der Broek *et al.*, 1979). Hence, the ordering is symmetrically preferable.

All substitutional atoms have atomic radii (r_i) larger than Fe or Ni in the L phase and the observed expansion of the c axis of the L phase from the c axis of FeNi is therefore expected. From r_{Ni} = 1.24, r_{Fe} = 1.26 and r_M = 1.30 Å the c axis of the L phase could be estimated as follows: 3.579 Å $(r_M + r_{Ni})/(r_{Fe} + r_{Ni})$ = 3.63 Å, which is entirely consistent with that determined by the experiment.

The stacking sequence in the $L1_0$ structure is ABC with a tetragonal unit in the closed-packed plane (Beattie Jr, 1967). The ABC stacking gives rise to the ordered $L1_0$ structure as shown in Fig. 7(a). The different orientation of the L phase can be present using the ABC stacking because the L phase has the $L1_0$ structure type. The lost rotation symmetry elements due to the ordering of the L phase from the f.c.c. structure with $Fm\overline{3}m$ should give rise to orientation variants of the L phase. The number of variants is given by the ratio of the order of the point group of the disordered f.c.c. and the order of the point group of the ordered L phase, namely [48(for |$m\overline{3}m$)]/[16(for $4/mmm$)] = 3 (Van Tendeloo & Amelinkx, 1974). The ordering in the close-packed plane could be any one of the three equivalent directions ⟨100⟩ in the f.c.c. and the resulting structure will then be related to each other by a rotation of 120°, as shown in Fig. 7. In other words, they are related by a twin relationship. Hence, the occurrence of microtwins or domains could explain the extra spots or streaking in the electron diffraction pattern as shown in Fig. 5(b). It is also noteworthy that the twin boundaries shown in Fig. 7 are non-conservative and, therefore, also non-conservative domain boundaries.

The present result has demonstrated the possibility of determining the crystal structure of a small crystal with the
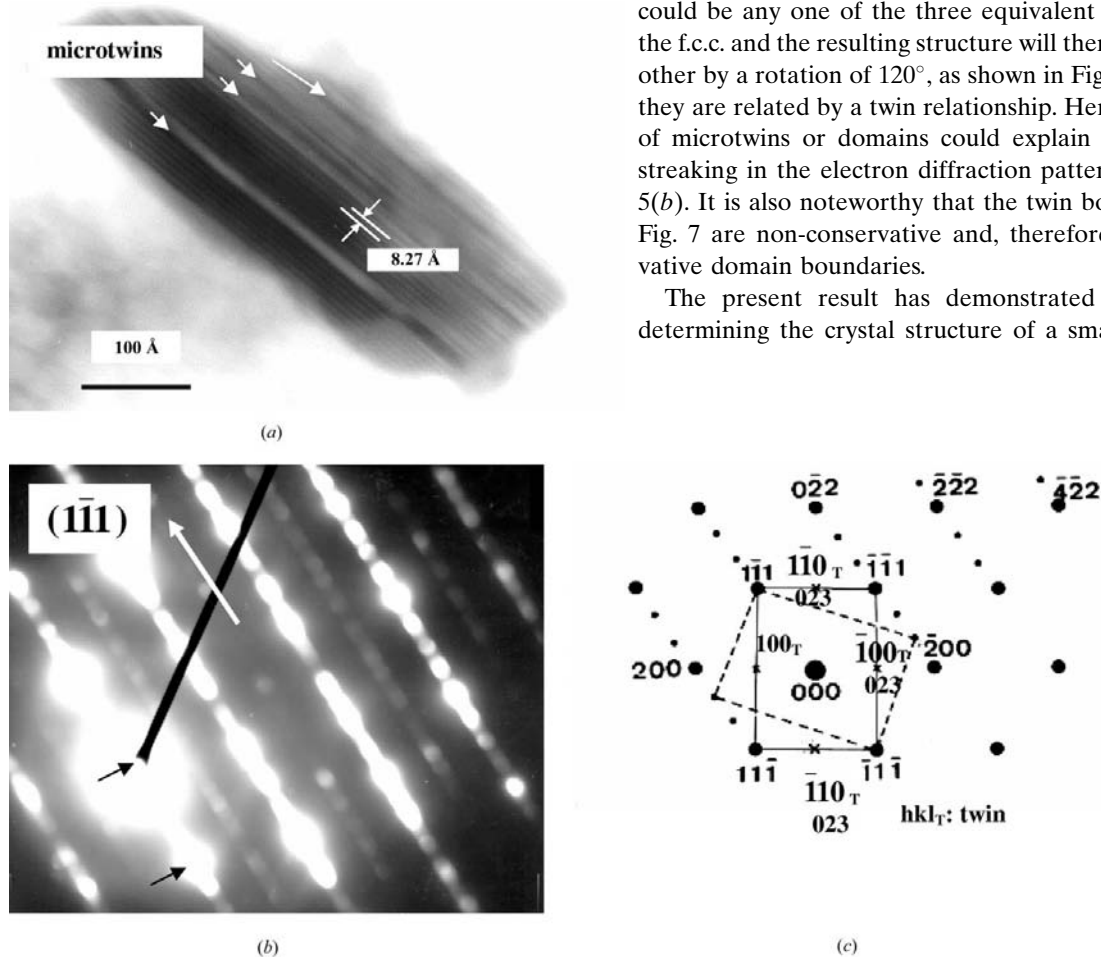

Figure 5
(a) High-resolution electron microscopy image (HREM) of an L-phase particle. (b) Small-angle CBED pattern from the [110] zone pattern. The white arrow indicates the twin direction while the black ones indicate the fundamental reflections. (c) The schematic solution of the pattern of the [110] zone pattern.

Table 3
The comparison between the calculated (I_{calc}) and experimental intensities (I_{exp}) for the electron diffraction.

* not obtained by experiment and therefore not included in R calculation.

hkl for cubic	d_{hkl} (Å)	I_{exp}	I_{calc}	$|I_{exp} - I_{calc}|$
001	3.6300	9.1	2.10	7.00
110	2.4890	14	1.85	12.15
111	2.0528	1000	1234.18	234.18
002	1.8150	311	202.41	108.59
200	1.7600	300	367.79	67.79
112	1.4665	1.8	0.99	0.81
202	1.2635	128	212.28	84.28
220	1.2445	88	101.20	13.20
003	1.2100	9	0.25	8.75
221	1.1772	8	0.74	7.26
310	1.1131	0	0.00	0.00
113	1.0882	320	129.59	190.41
311	1.0642	–	(245.60)*	–
222	1.0264	52	112.31	60.31
203	0.9971	2	0.99	1.01
312	0.9489	–	(2.22)	–
004	0.9075	57	25.92	31.08
400	0.8800	146	53.07	92.93
223	0.8675	–	(1.73)	–
401	0.8552	1.6	1.85	0.25
$\sum$		2447.5	2447.5	920.01

Figure 7
Three different orientations of ordering at the {111} projection which are twin-related. The primitive tetragonal unit cell was chosen and the boundaries indicated by dashed lines. Note they are non-conservative domain boundaries.

also be described using the primitive lattice type of $a = 2.49$ and $c = 3.63$ Å, $V = 22.5$ Å^3 and $Z = 1$. The density is ~ 6.98 g cm^{-3}.

dimensions $100 \times 500 \times 500$ Å using a combination of EDX analyses, CBED and HREM.

5. Conclusions

The L phase was observed after ageing at 748 and 823 K. It has a flake-like morphology with the dimensions $100 \times 200 \times 500$ Å. The structure of the L phase was determined using a combination of EDX analyses, electron diffraction and computer simulation.

The L phase was found to be isostructural to the ordered phase FeNi. The L phase could be described as Ti$_{19}$Fe$_9$Mo$_9$Al$_8$Cr$_5$Ni$_{50}$ or simply M_{50}Ni$_{50}$, or even MNi (M = Ti, Fe, Mo, Al and Cr). The structure of the L phase was determined to have the ordered structure of the CuAu-I type ($L1_0$, $P4/mmm$, $a = 3.52$, $c = 3.63$ Å, $V = 45.0$ Å^3 and $Z = 2$) with two Ni atoms at $\frac{1}{2}0\frac{1}{2}$ and $0\frac{1}{2}\frac{1}{2}$, and two M atoms at 000 and $\frac{1}{2}\frac{1}{2}0$. It can
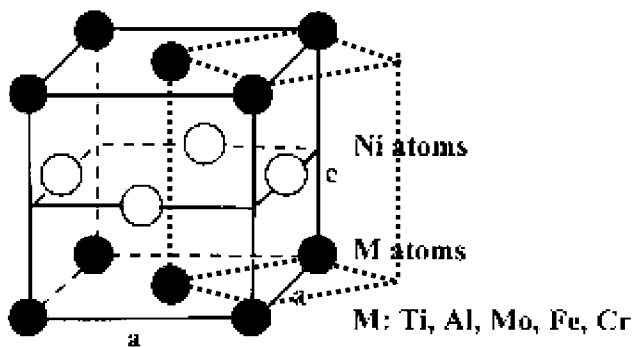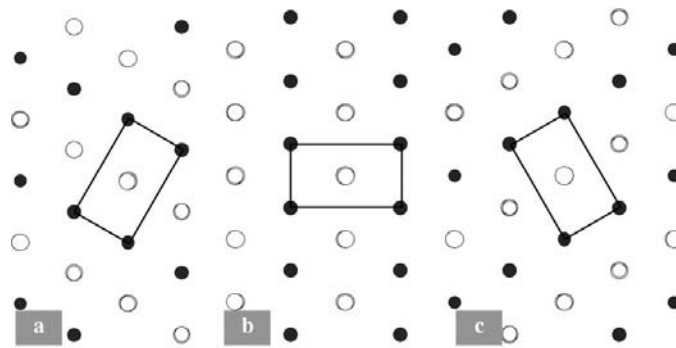

Figure 6
The atomic ordering in the L phase. Note that the dashed line indicates the choice of tetragonal unit cell.

References

Beattie Jr, H. J. (1967). *Intermetallic Compounds*, edited by J. H. Westbrook, pp. 144–165. New York: John Wiley and Sons.
Broek, J. J. van den, Donkersloot, H., Van Tendeloo, G. & Van Landuyt, J. (1979). *Acta Metall.* **27**, 1497–1504.
Buxton, B. F., Eades, J. A., Steeds, J. W. & Rackham, G. M. (1976). *Philos. Trans. R. Soc. A*, **281**, 15–194.
Cullity, B. D. (1978). *Elements of X-ray Diffraction*, 2nd ed., pp. 383–396. New York: Addison-Wesley Publishing Company Inc.
Danon, J., Scorzelli, R. B., Azevedo, I. S. & Imakuma, K. (1980). *Phys. Scr.* **21**, 223–224.
Deckers, R. F. & Floreen, S. (1988). *Maraging Steel: Recent Development and Applications*, edited by R. K. Wilson, pp. 1–38. Warrendale, PA: TMS-AIME.
Edington, J. W. (1975). *Electron Diffraction in the Electron Microscope*, Vol. 2, pp. 58–77. London: Macmillan Press Ltd.
Floreen, S. (1968). *Met. Rev.* **13**, 115–128.
Hultin Stigenberg, A. & Nilsson, J.-O. (1993). *Wire J. Int.* **26**, 62–69.
Kim, Y. G., Jung, J. Y., Park, C. N. & Lee, C. S. (1988). *Managing Steel: Recent Development and Applications*, edited by R. K. Wilson, pp. 107–123. Warrendale, PA: TMS-AIME.
Liu, P., Hultin Stigenberg, A. & Nilsson, J.-O. (1994). *Scr. Metall. Mater.* **31**, 249–254.
Sha, W., Cerezo, A. & Smith, G. D. W. (1993a). *Metall. Trans. A*, **24**, 1221–1232.
Sha, W., Cerezo, A. & Smith, G. D. W. (1993b). *Metall. Trans. A*, **24**, 1233–1239.
Sha, W., Cerezo, A. & Smith, G. D. W. (1993c). *Metall. Trans. A*, **24**, 1241–1249.
Vainshtein, B. K. (1981). *Modern Crystallography*, Vol. I, pp. 314–315. Berlin: Springer-Verlag.

Vainshtein, B. K., Fridkin, V. M. & Indenbom, V. L. (1982). *Modern Crystallography*, Vol. II, pp. 69–90. Berlin: Springer-Verlag.

Van Tendeloo, G. & Amelinkx, S. (1974). *Acta Cryst.* A**30**, 431–440.

Vasudevan, V. K., Kim, S. J. & Wayman, C. M. (1990). *Metall. Trans. A*, **21**, 2655–2668.

Villars, P. & Calvert, L. D. (1985). *Pearson's Handbook of Crystallographic Data for Intermetallic Phases*, Vol. 2, pp. 1612–1613. Metals Park, OH: American Society for Metals.

Viswanathan, U. K., Dey, G. K. & Asundi, M. K. (1993). *Metall. Trans. A*, **24**, 2429–2442.

Wilson, A. J. C. (1995). Editor. *International Tables for Crystallography*, Vol. C, pp. 223–244. Dordrecht: Kluwer Academic Publishers.

Zou, X. D., Sukharev, Y. & Hovmöller. S. (1993). *Ultramicroscopy*, **49**, 147–158.

Zou, X. D., Sukharev, Y. & Hovmöller. S. (1994). *Ultramicroscopy*, **52**, 436–444.